Uncertainties in models predicting critical bed shear stress of cohesionless particles

Emeline Perret, Benoit Camenen, Céline Berni, Kamal El Kadi Abderrezzak, Benjamin Renard

Uncertainties in models predicting critical bed shear stress of cohesionless particles

Emeline Perret[1,2], Benoit Camenen[3], Céline Berni[4], Kamal El kadi Abderrezzak[5], and Benjamin Renard[6]

[1]INRAE, UR RiverLy, centre de Lyon-Villeurbanne, 5 Rue de la Doua, CS 20244, F-69625 Villeurbanne Cedex, France.

[2]CNR, Compagnie Nationale du Rhône, 4 rue de Chalon-sur-Saône, 69007 Lyon, France. Email: e.perret@cnr.tm.fr

[3]INRAE, UR RiverLy, centre de Lyon-Villeurbanne, 5 Rue de la Doua, CS 20244, F-69625 Villeurbanne Cedex, France. Email: benoit.camenen@inrae.fr

[4]INRAE, UR RiverLy, centre de Lyon-Villeurbanne, 5 Rue de la Doua, CS 20244, F-69625 Villeurbanne Cedex, France. Email: celine.berni@inrae.fr

[5]EDF R&D, LNHE / LHSV, 6 Quai Watier, 78401 Chatou, France. Email: kamal.el-kadi-abderrezzak@edf.fr

[6]INRAE, UR RiverLy, centre de Lyon-Villeurbanne, 5 Rue de la Doua, CS 20244, F-69625 Villeurbanne Cedex, France. Email: benjamin.renard@inrae.fr

ABSTRACT

Our data show a large scatter for the critical Shields stress for initial sediment motion. The main sources of dispersion are related to the methodological procedures defining the inception of movement (i.e., visual observations or extrapolation of sediment transport rate) and to the estimation of the bed shear stress. The threshold for sediment motion varies with many factors related not only to grain size, but also with bed composition (e.g., presence of fine sediments in a coarse matrix), arrangement (e.g., bed roughness, grain orientation and characteristic lengths

of bed structures) and slope. New models to estimate the critical Shields number are proposed combining both grain size or/and bed slope. Model parameters and uncertainty are estimated through Bayesian inference using prior knowledge on those parameters and measured data. Apart from the uncertainty in observations, two types of uncertainty can be evaluated: one related to the parameter estimation (i.e., parametric) and one related to the choice of the model (i.e., structural). Eventually, a four-parameter model based on both the grain size and bed slope yields the best results and demonstrates a potential interaction between these two parameters. Model uncertainty remains, however, large, which indicates that other input parameters may be needed to improve the proposed model.

INTRODUCTION

Understanding sediment transport is a major concern in many fluvial and ecohydraulic studies (e.g., riverbed mobility, habitat, water quality) and predicting the critical conditions for incipient particle motion remains a fundamental and practical problem. Bedload increases rapidly and non-linearly with bed shear stress, and large uncertainties in predicting its rate near incipient motion have been observed in gravel-bed rivers (Camenen and Larson 2005; Recking et al. 2008; Camenen et al. 2011). Shields (1936) defined the dimensionless bed shear stress as:

$$\theta = \frac{\tau}{(\rho_s - \rho) g d} \tag{1}$$

with τ the bed shear stress, ρ_s and ρ the densities of sediment and water, respectively, g the acceleration of gravity, and d the grain size. The criterion for incipient motion of sediment particles is commonly expressed in terms of the critical Shields number θ_{cr}. Most sediment transport formulas, generally derived from laboratory experiments on well-sorted sediment mixtures, relate bedload rate q_{sb} to the excess bed shear stress $(\theta - \theta_{cr})$ (Meyer-Peter and Müller 1948; Parker et al. 1982; van Rijn 1984; Lajeunesse et al. 2010). The validity of these formulas may be questionable when applied to field cases, such as gravel bed rivers with poorly sorted sediment mixtures and complex bed features (Recking 2010). Accurate estimation of the bed shear stress and its critical

value for incipient motion is then challenging (Perret et al. 2020).

Buffington and Montgomery (1997) reported a large dataset for the critical Shields number and the Soulsby and Whitehouse (1997) equation provides a rough fit of θ_{cr} expressed in terms of the dimensionless grain size $d_* = d_{50}[g(s-1)/\nu^2]^{1/3}$ (with $s = \rho_s/\rho$ the relative sediment density, ν the kinematic viscosity of the fluid, and d_{50} the median grain size). Still, a significant scatter in the data exists, as for a given d_*-value, θ_{cr} can vary more than one order of magnitude. Data scatter may result from the experimental set-up conditions (e.g., initial bed arrangement) and from the methodological procedures used to define the concept of incipient motion and to compute θ_{cr} (Buffington and Montgomery 1997). The scatter in the data may also reflect that θ_{cr} depends not only on grain size (Garcia 2008) but also on bed slope (Recking 2009), hiding/exposure of grains (Wilcock and Crowe 2003), particle imbrication, and degree of clogging (Perret et al. 2018).

Several studies have put forward the dependence of the critical bed shear stress on bed arrangement (Tait 1993; Haynes and Pender 2007; Yager et al. 2018; Perret et al. 2020; Hassan et al. 2020; Hodge et al. 2020) which has been described through many indicators, such as the roughness height of grains, their shape (Lane and Carlson 1954; Li and Komar 1986; Petit 1989), emergence (Fenton and Abbott 1977), orientation and imbrication (Laronne and Carson 1976; Reid et al. 1980; Brayshaw et al. 1983), the degree of bed armouring, and the characteristic lengths of bed clusters/structures (Church et al. 1998; Venditti et al. 2017). Because the antecedent flow conditions impact the arrangement of the bed surface, θ_{cr} is thus related to the stress history (Haynes and Pender 2007). The critical Shields number of coarse particles can also vary by several percent (Perret et al. 2018) according to the proportion of matrix fines (cohesive or not) (Reid et al. 1985; Curran 2007; Jain and Kothyari 2009; Barzilai et al. 2013; Kuhnle et al. 2013; Wren et al. 2014; Perret et al. 2018), i.e., fine sand can increase bedload by lubrication, whereas the opposite effect is observed with silt and clay due to consolidation effect. Finally, hiding and exposure modify the critical Shields number for each size class in mixtures of non-cohesive sediment particles (Jackson and Beschta 1984; Ikeda and Iseya 1988; Wilcock and Crowe 2003; Curran 2007; Kuhnle et al. 2013; Wren et al. 2014; Perret et al. 2018). Nevertheless, the effects of hiding/exposure can be quantified

based only on a reference critical bed shear stress for unisized material or based on the median grain size - the focus of the present study.

Several have observed that θ_{cr} increases with mild slopes longitudinal bed slope S ($0.001 \leq S \leq 0.05$) (Shvidchenko and Pender 2000; Mueller et al. 2005; Lamb et al. 2008; Recking 2009). For very steep slopes ($S > 0.05$), Chiew and Parker (1994) demonstrated that θ_{cr} decreases with S. The reasons for the increase in θ_{cr} with $S \leq 0.05$ remains partially explored. When S increases, stable bed structures appear, leading to morphologic changes and less available shear stresses for bedload. The slope effect could in fact be a drag effect due to bed re-arrangement. However, detailed experiments by Shvidchenko and Pender (2000) with well-sorted materials indicate that bed arrangement cannot entirely explain the increase in θ_{cr}. Indeed, the slope effect can be associated with changes in relative roughness k_s/h, (with k_s the bed roughness height and h the flow depth), i.e., k_s/h increases with S (Lamb et al. 2008; Recking 2009; Camenen 2012). In a larger extent, the hydrograph can be related to the bed slope (steeper for high slopes) and flow acceleration may have an impact on friction, and thereby on bed shear stress (Camenen and Larson 2010). However, only steady flows will be considered in our study, in which case the slope effect can be regarded as a combination of at least the following two factors: bed arrangement and relative roughness. As the direct parameters describing bed arrangement are often not reported in previous studies, we explore bed arrangement only through the effect of bed slope on the critical shear stress.

This study aims at discussing the estimation of the critical Shields number θ_{cr} and associated uncertainty. The paper is organised as follows: Section 2 is a review of existing methodologies for computing bed shear stress and critical value for inception of motion. Data collection and three θ_{cr}-predictive models based on d_*, S or both are presented in Section 3 together with the Bayesian framework for uncertainty quantification. In Section 4, model parameters are estimated through Bayesian inference using prior knowledge on those parameters and observational data. The final estimation of θ_{cr} is then associated with a parametric uncertainty (related to the parameter estimation) and with a structural uncertainty (related to the choice of the model), which enables the evaluation of performance of the models. Results are discussed in Section 5, followed by

concluding remarks in Section 6.

SOURCES OF UNCERTAINTY IN MEASUREMENT OF CRITICAL BED SHEAR STRESS

Methods for bed shear stress computation

Various methods are available to compute the bed shear stress τ and most of them are reported in Table. 1 (see Supplementary material). The depth-slope equation for uniform flow yields a reach-averaged value for τ. The 1D Barré Saint-Venant equation (BSV) is preferred for non-uniform and unsteady flows. Friction laws calculate τ from the depth-averaged velocity (locally measured) or the cross-sectional-averaged velocity. Local bed shear stresses can also be estimated based on velocity profile measurements using either time-averaged values or fluctuations (Wilcock 1996; Biron et al. 2004). Different τ values (Shields number θ values) probably can be obtained depending on the chosen method. Those differences may explain a part of the scatter in the data of the critical Shields number.

Field studies demonstrate that the bed shear stress calculated from the depth-slope equation is generally larger than the one computed from the analysis of velocity profile (Petit 1989). The first method provides a value at the cross-sectional scale τ_t that lumps several components of flow friction such as the grain resistance τ', which is responsible for inception of motion and bedload transport, and the bedform resistance τ'' (i.e., $\tau_t = \tau' + \tau''$). On the contrary, the velocity profile method yields the local bed shear stress, which can be assimilated to τ'. In most existing studies, indication about bedforms are almost missing; τ'' remains difficult to estimate and can represent $10 - 75$ % of τ_t (Buffington and Montgomery 1997). According to Petit et al. (2005), an uncertainty of 50 % can be obtained for θ_{cr} if the calculation is based on the total bed shear stress τ_t.

The major source of uncertainty for the depth-slope equation is mainly due to the estimation of the energy slope. For laboratory cases, the flume can even be too short to observe a water elevation gradient larger than the precision of the measuring device. In field cases, the depth-slope method is often improperly used, leading to large uncertainty, e.g., when the flow is not uniform or by replacing J and R_h by S and h, respectively.

One of the main difficulties using local methods in small scale laboratory experiments is to define the flow depth h related to the reference bed level z_b, especially for coarse sediments for which a spatial variability does exist even if the bed is flat. Wilcock (1996) found that measurement uncertainty related to the velocity profile analysis and friction law methods was 5 % and between $5-15$ %, respectively. Biron et al. (2004) ranked the Reynolds stress analysis as the most accurate method for beds with no forms and specific grain arrangement. For complex beds, the turbulent kinetic energy method (TKE) was recommended (Kim et al. 2000). For velocity profile and friction law methods, one major issue is the definition of the roughness length Z_0 .

Definition of incipient motion

One of the main issues related to bedload is the definition of incipient motion. Some exhaustive reviews (Lavelle and Mofjeld 1987; Dey 1999; Beheshti and Ataie-Ashtiani 2008) can be classified in two main categories. The first one is based on sediment flux: the measured bedload rate q_s is extrapolated to zero (Shields 1936), or to a low reference value $q_{s,ref}$ (U. S. Waterways Experiment Station 1935); the associated bed shear stress refers to incipient motion (i.e., critical bed shear stress). The Shields (1936) method was contested, as sediment motion was measured at conditions below the Shields diagram, which was attributed to fluctuating instantaneous velocities (Paintal 1971). Consequently, it may be more appropriate to consider a bed shear stress that yields a minimum transport rate to determine the incipient motion - $q_{s,ref} = 1.6 \times 10^{-7}$ m^2/s (U. S. Waterways Experiment Station 1935). Using a dimensional flux is, however, highly sensitive to the type and size of sediment particles: one single gravel particle in motion (representative diameter $d \geq 1$ cm) is sufficient to exceed the U. S. Waterways Experiment Station (1935) reference bedload rate criteria, whereas around 1000 particles are needed if $d = 1$ mm. Following Einstein (1942)'s definition, the use of an arbitrary dimensionless transport rate $q_s^* = q_s/(\sqrt{(s-1)gd^3}$ improves the results but remains grain size-dependent. Parker et al. (1982) related the incipient motion to a low dimensionless transport rate $W_{ref}^* = q_s^*/\theta^{3/2} = 0.002$, but this criterion is adapted to sand particles.

The second category is based on visual observations. The flow discharge (i.e., bed shear stress) is increased progressively until movement of particles is detected. Several have used this method

for laboratory experiments, but applied their own definition for the incipient motion (Kramer 1935; Vanoni 1964). Conducting experiments on a mixture of poorly sorted sand, Kramer (1935) proposed the following four levels of sediment transport: (i) No transport, (ii) Weak transport - few of the smallest particles are in motion at isolated spots, (iii) Medium transport - particles of mean diameter are in motion at a small rate; and (iv) General transport - all particles are moving at all spots and at all times over the bed. Recking et al. (2008) merged the second and third levels. Kramer (1935) defined the threshold of motion to be the bed shear stress yielding general transport. The main difficulty of the visual method is the distinction between the above levels. Vanoni (1964) defined the threshold of incipient motion as the condition under which at least one grain is in movement every two seconds at any location. Neill and Yalin (1969) proposed a similar definition based on a dimensionless parameter $\epsilon = (n\Delta t/A)[\rho d^5/(\rho_s - \rho)g]^{1/2}$, where n is the number of moving particles during a given time of observation Δt on an observed bed area A. According to Neill and Yalin (1969), $\epsilon = 10^{-6}$ corresponds to the inception of movement (≈ 0.8 grain/m^2/s). One issue remains: the validity of such criteria for any grain size.

These concepts of sediment threshold leads to a large scatter in the dataset and make comparisons difficult. It is obvious that there is no equivalence between the existing definitions. For example, both Vanoni (1964)'s definition and U. S. Waterways Experiment Station (1935)'s criterion do not reflect the same amount of transport rate: for $d = 3$ mm, Vanoni's definition yields $q_{s,ref} \approx 10^{-8}$ m^2/s ($q_{s*,ref} \approx 2 \times 10^{-5}$), whereas USWES's criterion yields $q_{s*,ref} = 1.6 \times 10^{-7}$ m^2/s ($q_{s*,ref} \approx 2.5 \times 10^{-4}$).

Evaluation of uncertainty in measurements of critical Shields number

It is possible to attribute an estimation of uncertainty to each data point θ_{cr} according to two uncertainty sources: definition of threshold for sediment motion (Δ_{def}) and methodology for computing bed shear stress (Δ_τ). The final uncertainty on θ_{cr} can be written as follows:

$$\Delta\theta_{cr} = \frac{u_{\theta_{cr}}}{\theta_{cr}} = \sqrt{\Delta_{def}^2 + \Delta_\tau^2} \tag{2}$$

Table 2 recaps the proposed uncertainties according to the type of data based on expertise and literature. Note that the focus should not be on uncertainty values but rather on how they can be compared to each other. Most values in Table 2 were evaluated during marginal flume tests carried out for Perret (2017) study where critical Shield numbers were estimated with the different methods and definitions. The other values were assumed based on literature review (see Sections 2 and 2).

Uncertainty for field data is expected to be larger than for laboratory data, partly because in-situ measurements are more difficult to achieve, grain size distributions are poorly sorted and often spatially distributed, and cross-sections are irregular with possible bedforms. Also, since field measurements are often achieved over large periods, the studied river section may encounter bed changes. It should be noted that most data based on field experiments used here are from Mueller et al. (2005), who used Parker et al. (1982)'s criteria and depth-slope method.

As explained in Section 2, using a reference transport rate as an incipient motion definition is more robust than a visual definition ($\Delta_{def1} < \Delta_{def2}$, subscripts *def1* and *def2* correspond to reference transport rate definition and visual definition, respectively). Using the reference transport rate, the uncertainty lies mainly in the arbitrary chosen value for the reference transport rate but also in the reliability of measurements. For example, data collected with a Helley-Smith sampler and averaged throughout the river cross-section can lead to significant uncertainties (Vericat et al. 2006; Liu et al. 2008). For laboratory experiments, bedload transport is often measured using a scale positioned at the downstream end of the flume (Aguirre-Pe et al. 2003; Perret 2017). The uncertainty Δ_{def1} is evaluated thus equal to 10 %. For field experiments, since bedload transport is usually measured partially by sampling a finite number of points throughout the river section, we evaluate $\Delta_{def1} = 20\%$. For laboratory data, we propose an uncertainty using the visual definition $\Delta_{def2} = 15$ % based on Perret (2017)'s experiments. This was recently confirmed by Vah et al. (2022), who observed that the visual definition generally leads to lower critical bed shear stress compared to other methods. Visual definition is generally not used for field data. There exists a data set from Young and Mann (1985) for which inception of motion was revealed by photo analysis. We set the uncertainty for this case at 30%.

Uncertainty associated to the depth-slope method for bed shear stress computation is set for field experiments at 25 %, as the bed slope is generally used instead of the free surface slope and water depth may vary significantly throughout the river cross-section. These values are lower for laboratory studies, where bed conditions are constrained by the flume. The uncertainty for flume study $\Delta_{\tau,DS}$ is mainly linked to the calculation of the energy slope; we suggest $\Delta_{\tau,DS}$ =15%. This uncertainty may increase for specific cases with relatively coarse sediments and low water depths for which the spatial variability of the water depth is higher. Uncertainties for the other local methods vary according to the topographic complexity of the studied zone (see Section 2). Local techniques require many measurement points to evaluate a spatial and time-averaged bed shear stress. The presence of poorly sorted sediments makes also difficult the evaluation of the roughness length and bed level. Such local measurements are less common in the field. The proposed values in Table. 2 are based on Perret (2017)'s experiments.

MATERIAL AND METHODS

Data compilation

We compiled an up-to-date data set for the estimation of θ_{cr}. It includes the data collected by Buffington and Montgomery (1997) but excluding data that used the competence function or theoretical developments. Indeed, the latter have not really been validated and lead to substantially different results compared to those obtained by the other methods. It also includes additional data collected by Recking (2009) as well as some additional data from the following studies : Rao and Sitaram (1999), Gregoretti (2000), Shvidchenko et al. (2001), Pilotti and Menduni (2001), Dey and Raju (2002), Dancey et al. (2002), Aguirre-Pe et al. (2003), Mueller et al. (2005), Hoffmans (2010), Prancevic and Lamb (2015), Roušar et al. (2016), Perret et al. (2020). The final data set includes 921 points (329 points obtained with the bedload extrapolation definition, and 592 points obtained wih the visual method). Most of these data are from laboratory experiments (867 points). The 54 points corresponding to field measurements were mostly obtained from Mueller et al's (2015) study using coupled measurements of flow and bed load transport in 45 gravel-bed streams and rivers in western North America. Even if flumes represent a small patch of the temporal and spatial

variability of a natural river that can also be biased due to scale effects, they remain of interest to study bedload transport processes since they provide data for controlled conditions with reduced uncertainties.

The measurement uncertainties $\Delta\theta_{cr}$ were estimated for each data point based on values reported in Table 2. Consequently, we obtained $\Delta\theta_{cr} = 21\%$ for laboratory data using the reference transport rate definition, $\Delta\theta_{cr} = 25\%$ for laboratory data using the the visual definition, and $\Delta\theta_{cr} = 35\%$ for field data (using the the reference transport rate definition). Since most of the data are from laboratory experiments, we eventually have an averaged value $\overline{\Delta\theta_{cr}} = 25$ %. Figure 1 presents the uncertainty $u_{\theta_{cr}}$ as a function of the dimensionless grain size d_*. The largest values are observed for very fine and very coarse sediments since θ_{cr} can be over 0.1 for these specific grain sizes.

Tab. 2 here.

Fig. 1 here.

Again, this evaluation of the measurement uncertainties in data corresponds to a first rough estimation. The impact of the choice for $\Delta\theta_{cr}$ on the results is discussed in Section 5 using a sensitivity analysis.

Models for estimating θ_{cr}

We propose here to test simple models for the estimation of the critical Shields number for inception of movement. First, we assumed the Shields curve can be evaluated as a function of the grain size only (through the input parameter d_*) based on the equation of Soulsby and Whitehouse (1997):

$$\widehat{\theta}_{cr}^{(1)} = \frac{\nu_1^{(1)}}{d_*} + \nu_2^{(1)} \left[1 - \exp(\nu_3^{(1)} d_*)\right] \tag{3}$$

where $\widehat{\theta}_{cr}^{(k)}$ is the critical Shields number predicted by the model k (here $k = 1$), $\nu_1^{(1)}$, $\nu_2^{(1)}$, and $\nu_3^{(1)}$ are the parameters to evaluate ($\nu_1^{(1)} = 0.24$, $\nu_2^{(1)} = 0.055$, and $\nu_3^{(1)} = -0.02$ according to Soulsby

and Whitehouse (1997)). The Soulsby and Whitehouse (1997) equation was chosen since it is a continuous, single equation suitable for all grain size while including three fitting parameters only. As compared to other formulas describing the empirical Shields curve as a function of the grain size (Iwagaki 1956; van Rijn 1984), the Soulsby and Whitehouse (1997) equation yields very similar results. Some difference appears for the extrapolation for very fine sediments for which there is a lack of data for non-cohesive sediments. We assume a critical bed shear stress independent of the grain size as proposed by Soulsby and Whitehouse (1997).

Following the same idea, the critical Shields parameter can be evaluated as a function of the bed slope only, based on Recking (2009) equation:

$$\widehat{\theta}_{cr}^{(2)} = \nu_1^{(2)} S + \nu_2^{(2)} \tag{4}$$

where $\nu_1^{(2)}$ and $\nu_2^{(2)}$ are the parameters to evaluate ($\nu_1^{(2)} = 0.3$ and $\nu_2^{(2)} = 0.04$ according to Recking (2009)).

We propose to use a combination of Eqs. 3 and 4 to evaluate the critical Shields parameter as a function of both grain size and slope:

$$\widehat{\theta}_{cr}^{(3)} = \left(\nu_1^{(3)} S + \nu_2^{(3)}\right) \times \left(\frac{\nu_3^{(3)}}{d_*} + \nu_4^{(3)} \left[1 - \exp(\nu_5^{(3)} d_*)\right]\right) \tag{5}$$

where $\nu_1^{(3)}$, $\nu_2^{(3)}$, $\nu_3^{(3)}$, $\nu_4^{(3)}$, and $\nu_5^{(3)}$ are the parameters to evaluate. Eq. 5 is an adjustment of Eq. 3 with an additional slope parameter. Eq. 5 is close to the following equation proposed by Camenen (2012):

$$\begin{aligned} \widehat{\theta}_{cr} = \; & \left(0.5 + 6S^{0.75}\right) \frac{\sin(\phi_s - \arctan S)}{\sin(\phi_s)} \\ & \left(\frac{0.24}{d_*} + 0.055 \left[1 - \exp(-0.02 d_*)\right]\right) \end{aligned} \tag{6}$$

where ϕ_s is the angle of repose of sediment. It should be noted that Eq. 5 does not include the possible instability due to steep slopes as Eq. 6 does. However, our data set is limited to bed slopes below 30% , above which the term $\sin(\phi_s - \arctan S)/\sin(\phi_s)$ starts to be significant.

Bayesian estimation of predictive models

Overview and inference setup

Several sources of uncertainty affect the use of models in Eqs. (3-5). First, their parameters $\nu_i^{(k)}$ are unknown and will remain uncertain even after model calibration (parametric uncertainty). Second, model calibration makes use of observed θ_{cr} that are uncertain as described in section 3 (observation uncertainty). Finally, the models are not perfect and are not expected to exactly replicate θ_{cr} (structural uncertainty).

Bayesian estimation provides a general and rigorous mechanism to estimate the unknown parameters of a model. It combines the information brought by uncertain calibration data with any pre-existing 'prior' information on the parameters. The method used in this paper is presented in details by Le Coz et al. (2014), Mansanarez et al. (2016), and Perret et al. (2021). It was initially implemented for hydrometric rating curves but it can be applied to any kind of models.

Let $\boldsymbol{O} = \left(d_{*,i}, S_i, \theta_{cr,i}, \Delta_{\theta_{cr},i}\right)_{i=1,\dots,n}$ denotes the n observations in the dataset described in section 3. Each observation vector comprises values for grain size, slope, critical bed shear stress and its uncertainty (as described in section 2).

In addition, let M denotes any of the models proposed in equations (Eqs. 3-5) to estimate a critical Shields number $\widehat{\theta}_{cr}$ from grain size d_* and/or slope S, with parameters $\boldsymbol{\nu}$:

$$\widehat{\theta}_{cr} = M\left(d_*, S; \boldsymbol{\nu}\right) \tag{7}$$

Bayesian estimation of parameters $\boldsymbol{\nu}$ requires two ingredients: an error model, linking an observed value $\theta_{cr,i}$ with the value $\widehat{\theta}_{cr}$ predicted by the model, and a prior distribution quantifying what is known about the parameters prior to having observed the data. This is illustrated by Figure 2.

Fig. 2 here.

Error model

The following error model is used to link observed and predicted values of θ_{cr}:

$$\theta_{cr,i} = \underbrace{M\left(d_{*,i}, S_i; \boldsymbol{\nu}\right)}_{\widehat{\theta}_{cr,i}} + \delta_i + \varepsilon_i \tag{8}$$

This equation describes two distinct error sources. The error δ_i is a measurement error and is assumed to be a realization from a Gaussian distribution with zero mean and known standard deviation $\Delta_{\theta_{cr},i}$ as described in section 2. The error ε_i is a structural error due to the imperfection of the model M. It is also assumed to be a realization from a Gaussian distribution with zero mean. However, its standard deviation σ is unknown, and therefore needs to be estimated along with parameters $\boldsymbol{\nu}$. The reason behind this distinct treatment of observation and structural errors is that the former exists independently of any model, and its properties can therefore be estimated beforehand. By contrast, the structural error is relative to the model of interest, and it is therefore difficult to know its properties before model estimation. Note that the normality of both measurement and structural errors is an assumption that can be evaluated through parameter estimation by examining residuals (i.e., observed minus predicted values). This assumption was found to be adequate for the data and models analysed in this work (not shown).

Prior distributions

For each unknown parameter, prior knowledge is encoded in a Gaussian distribution $\mathcal{N}(m, s)$. The mean value m represents a 'prior guess' and the standard deviation s represents the uncertainty around this prior guess. This standard deviation could potentially be very large when little is known about the parameter. In this paper, we choose to use as prior guess the values proposed by Soulsby and Whitehouse (1997) and Recking (2009) for Eqs. 3 and 4. For Eq. 5, prior guess values were evaluated assuming Eq. 5 corresponds to an adjustment of Eq. 3 using the additional slope parameter; so the prior guess values for parameters related to grain size were chosen equal to those of Eq. 3. Depending on the sensitivity on each of these parameters, a standard deviation was given between 30 and 50%. All prior guess values and related standard deviation are presented in Tab. 3

Tab. 3 here.

Outcome of Bayesian estimation

The raw outcome of Bayesian estimation is the posterior distribution of unknown parameters $(\boldsymbol{\nu}, \sigma)$. The probability density function (pdf) of this posterior distribution can be computed as shown in Appendix II. However, the posterior pdf is multi-dimensional and is therefore not easy to manipulate. Instead, it is more convenient to simulate many values from the posterior distribution, representing the posterior uncertainty in parameters. This simulation can be achieved by means of a Markov Chain Monte Carlo (MCMC) sampling algorithm. The particular sampler used in this paper is described in details in Renard et al. (2006).

Once many values $\left(\boldsymbol{\nu}_j, \sigma_j\right)_{j=1,\ldots,N_{sim}}$ have been simulated by MCMC, the uncertainty in critical bed shear stress can be quantified by propagating these simulated values through the model: this corresponds to the Monte Carlo propagation method described in uncertainty analysis standards (JCGM 2008). In particular, applying the model equation (Eq. 7) N_{sim} times yields N_{sim} values of $\widehat{\theta}_{cr}$ that represent parametric uncertainty, i.e., the uncertainty due to the imperfect estimation of parameters $\boldsymbol{\nu}$. The total uncertainty is obtained by adding to each of these N_{sim} values a structural error ε randomly sampled from a Gaussian distribution with zero mean and standard deviation σ_j. Note that measurement errors are not propagated at this stage, since the objective is to estimate the true θ_{cr}, rather than an observed, error-affected one. However, measurement errors still play an indirect role by affecting the posterior distribution and hence the uncertainty in estimated parameters.

RESULTS: ANALYSIS OF CRITICAL SHIELDS NUMBER UNCERTAINTIES

Evaluation of total uncertainty on critical Shields number using grain size only

Figure 3 plots the estimated $\widehat{\theta}_{cr}^{(1)}$ and related uncertainties using Eq. 3. Uncertainty bars of each data point are not plotted for the sake of readability. The best fit for Eq. 3 is obtained with $\nu_1^{(1)} = 0.196$, $\nu_2^{(1)} = 0.0405$, and $\nu_3^{(1)} = -0.0352$. Although lightly differING from the Soulsby

and Whitehouse (1997) equation, the final equation yields relatively similar results compared to the scatter in the experimental data points.

Fig. 3 here.

As shown in Fig. 3, the total uncertainty originates mainly from the structural error and can be enclosed between −60% and +60%. The chosen model is certainly not the most appropriate one, i.e., θ_{cr} is not only function of the parameter d_*. A more appropriate model would yield a dominance of parametric errors, meaning that the uncertainty comes mainly from data.

Evaluation of total uncertainty on critical shields number using bed slope only

Figure 4 presents the results obtained for the $\widehat{\theta}_{cr}^{(2)} = f(S)$ relationship and related uncertainties. Here, the best fit for Eq. 4 is obtained with $\nu_1^{(2)} = 0.327$ and $\nu_2^{(2)} = 0.0352$, which is quite close to the results from Recking (2009) ($\nu_1^{(2)} = 0.3$ and $\nu_2^{(2)} = 0.04$). Again, the total uncertainty comes mainly from the structural error and can be enclosed between −55% and +50%. For steep slopes ($S > 0.1$), the total uncertainty is lower and can be enclosed between −25% and +30%; the parametric error is no more negligible, meaning the model is more accurate here.

Fig. 4 here.

Evaluation of total uncertainty on critical shields number using both grain size and bed slope

Figure 5 depicts the results obtained for $\widehat{\theta}_{cr}^{(3)} = f(d, S)$ relationship and related uncertainties. The best fit for Eq. 5 is obtained with $\nu_1^{(3)} = 1.055$, $\nu_2^{(3)} = 0.274$, $\nu_3^{(3)} = 0.510$, $\nu_4^{(3)} = 0.134$, and $\nu_5^{(3)} = -0.068$. These values are quite different to our prior guess, but this is not surprising, since we assumed the slope to be an adjustment coefficient of the critical bed shear stress evaluated as a function of d_*. Interestingly, the curve for the range $3 < d_* < 40$ (i.e., sand-sized particles) is smoothed; the impact of grain size on the critical Shields parameter appears to be simpler than estimated from the Shields curve, i.e., inversely proportional to $d_*$for $d_* < 3$, and independent of d_* for $d_* > 40$. Indeed, most of data with sand particles were collected in low slope channels

whereas those with gravel particles correspond to larger slopes. A fit without accounting for the slope effects is thus biased by the data collection.

Fig. 5 here.

In Fig. 5 are presented results for four specific slopes: $S = 0.001$, $S = 0.02$, $S = 0.1$, and $S = 0.2$. The plotted experimental data correspond to slope values of the same order (±25%); they are plotted with their uncertainties. Compared to Fig. 3, the total uncertainty is slightly reduced and can be enclosed between −50% and +50%. The total uncertainty is still dominated by the structural error. However, the parametric error becomes less negligible for highest slopes. It should be noted, however, that the proposed model underestimates θ_{cr} values for steep bed slopes, which could be due to the relatively low number of data describing high slopes.

Performance of models

Table 4 presents the statistical results of the predictive capabilities of the different equations (see graphs in Appendix III). $E_{r,20}$ and $E_{r,50}$ correspond to a percentage of data predicted accurately with allowed error of a factor 1.2 and 1.5, respectively; mean_{log} and std_{log} correspond to the mean and standard deviation of the logarithm of the ratio between the predicted and measured value. It can be observed that the Bayesian inference leads to better predictive performances for Eqs. 3 and 4 since calibrated to the present larger data set as compared to the original calibration. A formulation with five parameters (Eq. 5) does not significantly improve the results apart for the standard deviation. When comparing measured to predicted θ_{cr}-values (see Figs. 8 and 9), one can observe that all formulas (apart from the Camenen (2012) formula, which presents a larger scatter) yield relatively constant values, while observations vary a lot. This suggests that grain size and slope are not the only parameters to consider for predicting the inception of transport.

Tab. 4 here.

It is interesting to note that statistics presented in Tab. 4 slightly differ if we consider laboratory data or field data only (see also Tab. 5). The dispersion is higher for field data than for laboratory

data, as expected but the mean_{log} are also higher suggesting that θ_{cr}-values are found smaller in the field. Field data correspond generally to poorly sorted sediments. The median grain size may be not adapted or sufficient to characterize the inception of motion of the mixture. Recking (2009) suggested using d_{84} instead of d_{50} for poorly sorted sediments. However, the fine sediment fraction may be the key parameter for reducing the critical bed shear stress (Wilcock 1988). In a similar way, the visual observation definition yields in general smaller θ_{cr}-values than the reference transport rate definition (Vah et al. 2022). This confirms the discussion in Section 2 and our suggestion to use a larger uncertainty for these data.

DISCUSSION

Assessment of retained data uncertainty

In Section 2, we attempted to evaluate uncertainty related to the technical sources for the critical Shields number data set. However, values in Table 2 remain partially subjective and arguable. A sensitivity analysis is performed to identify the impact of the choice of the uncertainty values on the results. We therefore explore the results obtained for a reduced (by a factor 1.3 and a factor 2) or an increased (by a factor 1.3 and a factor 2) data uncertainty. These changes would lead to an average data uncertainty $\overline{\Delta\theta_{cr}}$ of 12 %, 19 %, 32 % or 50 %, respectively. Let's remind that the averaged uncertainty initially was estimated at 25 %.

Fig. 6 shows the variation on the total and parametric uncertainties (E_{tot} and E_{par}, respectively) evaluated as an averaged of the ratio between the envelopes 97.5 % and 2.5 % for each d-values. Consequently, an absence of uncertainty would yield the value of 1. The total uncertainty clearly decreases with an increase in the data uncertainties since the latter explains a larger part of the residual scatter. On the other hand, a minima for the parametric uncertainty is observed for data uncertainties between 19 and 25 %. With a lower data uncertainty, the models are too restricted and unable to properly fit the data. With a larger data uncertainty, the estimated parameters of the models are too uncertain. This uncertainty value between 19 and 25% corresponds to an optimum to evaluate the parameters of the model. This is consistent with our first evaluation of the data average uncertainty (i.e., $\overline{\Delta\theta_{cr}}$ = 25 %).

Fig. 6 here.

For each equation (Eqs. 3, Eq. 4, and Eq. 5), we also tested the impact of the data average uncertainty $\overline{\Delta\theta_{cr}}$ on the model coefficient estimation (see Fig. 10). Results are highly sensitive to the specified data uncertainty. In particular, for Eq. 5, our choices of priors significantly affect results for large data uncertainties. Indeed, we assumed the slope term ($\nu_1^{(3)} S + \nu_2^{(3)}$) as a correction of Eq. 3 (with $\nu_2^{(3)} = 1$ as an initial prior) whereas the Bayesian approach indicates something intermediate : the posterior distribution of $\nu_2^{(3)}$ is three times narrower than its prior whereas the posterior distributions of $\nu_3^{(3)}$ and $\nu_4^{(3)}$ are three times wider than their prior. This would suggest that slope and grain size effects are competing each other.

A simple model for critical shields number using both grain size and slope

As the combination of slope and grain size effects reduce the smallest values observed for sand-sized particles, we propose to evaluate the critical Shields parameter as a function of both grain size and slope using the following four parameter equation:

$$\widehat{\theta}_{cr}^{(4)} = \left(\nu_1^{(4)} S + \nu_2^{(4)}\right) \times \left(\frac{\nu_3^{(4)}}{d_*} + \nu_4^{(4)}\right) \tag{9}$$

where $\nu_1^{(4)}$, $\nu_2^{(4)}$, $\nu_3^{(4)}$, and $\nu_4^{(4)}$ are parameters to evaluate. Since Eq. 5 is very similar to Eq. 9, we use the same priors, i.e., $\nu_1^{(4)} = 0.3$, $\nu_2^{(4)} = 1$, $\nu_3^{(4)} = 0.24$, $\nu_4^{(4)} = 0.055$. The best fit for Eq. 9 is obtained with $\nu_1^{(4)} = 1.158$, $\nu_2^{(4)} = 0.180$, $\nu_3^{(4)} = 0.410$, $\nu_4^{(4)} = 0.195$.

In Fig. 7 are presented results for four specific slopes: $S = 0.001$, $S = 0.02$, $S = 0.1$, and $S = 0.2$ in a similar way as in Fig. 5 for Eq. 5. Uncertainties are not improved compared to Fig. 5; they are enclosed between −55% and +55%. Nevertheless, when comparing to data, it clearly indicates there is no need of using such a complex empirical function of the grain size combined with the bed slope (Eq. 5). In addition, the simplified equation (Eq. 9) yields the best predictive performance compared to the other models with more than 70 % of the data predicted accurately with an allowed error of a factor 1.5 as shown in Table 4.

Fig. 7 here.

CONCLUSION

A series of equations was proposed to estimate the critical Shield number with an evaluation of its uncertainty. The models were derived from classical equations for the inception of movement relating the critical Shields number to grain size, or to longitudinal bed slope, or both. A Bayesian approach was used to estimate the model parameters using prior knowledge and observational data collected in literature. The Bayesian framework takes into account the measurement errors of the critical Shields numbers for the computation and gives two resulting uncertainty : a parametric (i.e., related to parameter estimation) and a structural (i.e., related to model itself) uncertainty. The main sources of measurement errors were reported and discussed, especially those related to the definition of the inception of motion and to the method used to compute bed shear stress. Measurement uncertainty was evaluated to 25 % in average for our data set. A sensitivity analysis was performed to discuss and verify this assumption by examining the impact of a reduced or increased measurement error on the results. Eventually, the proposed model (Eq. 9) improved results for estimating the critical bed shear stress for well-sorted sediments compared to existing models. However, for poorly-sorted sediments, one should use this model with the median grain size and apply additional laws for hiding and exposure effect.

A parametric uncertainty of approximately 10 % was found for θ_{cr} computed with models based on grain size or based on bed slope only. Total uncertainty was always larger than 50 %, which indicates significant structural uncertainty. A combination of both equations provided slightly better results. It also showed that smaller θ_{cr} values observed by Shields (1936) for sand particles may be a bias linked to the combination of grain size and slope effects. Eventually, a model based on four parameters and assuming a continuous decrease in θ_{cr} with an increasing grain size yields the best results. Significant uncertainty remains; the parametric uncertainty being always smaller than the structural uncertainty. This indicates that the grain size and the bed slope are insufficient to describe the inception of movement. A more accurate estimation of the inception of motion should integrate

other factors, such as parameters describing bed composition (presence of fine sediments in a coarse matrix) and bed arrangement (including bed roughness, grain orientation and characteristic lengths of bed structures) as suggested by Perret et al. (2020). However, such parameters were not measured in existing experiments, which limits the development of new predictive models.

Data availability statement

All data, models, or code that support the findings of this study are available from the corresponding author upon request.

Acknowledgments

This study has been supported by INRAE (formerly Irstea), the Rhône-Alpes region through the CMIRA ExploraPro financial support (B. Camenen), and the French National Research Agency (ANR) under the grant ANR-18-CE01-0019-01 (DEAR project), and EDF (Ph.D thesis of E. Perret). We would like to thank Alain Recking and Ladislav Roušar for providing their data sets.

REFERENCES

Aguirre-Pe, J., Olivero, M. L., and Moncada, A. T. (2003). "Particle densimetric froude number for estimatingsediment transport." *Journal of Hydraulic Engineering*, 129(6), 428–437.

Barzilai, R., Laronne, J. B., and Reid, I. (2013). "Effect of changes in fine-grained matrix on bedload sediment transport in a gravel-bed river.." *Earth Surface Processes & Landforms*, 38, 441–448.

Beheshti, A. A. and Ataie-Ashtiani, B. (2008). "Analysis of threshold and incipient conditions for sediment movement." *Coastal Engineering*, 55(5), 423 – 430.

Biron, P., Robson, C., Lapointe, M. L., and Gaskin, S. J. (2004). "Comparing different methods of bed shear stress estimates in simple and complex flow fields." *Earth Surface Processes & Landforms*, 29, 1403–1415.

Brayshaw, A. C., Frostick, L. E., and Reid, I. (1983). "The hydrodynamics of particle clusters and sediment entrainment in coarse alluvial channels." *Sedimentology*, 30, 137–143.

Buffington, J. M. and Montgomery, D. R. (1997). "A systematic analysis of eight decades of incipient motion studies, with special reference to gravel-bedded rivers." *Water Resources Research*, 33(8), 1993–2029.

Camenen, B. (2012). "Discussion of "understanding the influence of slope on the threshold of coarse grain motion: Revisiting critical stream power" by C. Parker, N.J. Clifford, and C.R. Thorne." *Geomorphology*, 139-140, 34–38.

Camenen, B., Holubová, K., Lukač, M., Le Coz, J., and Paquier, A. (2011). "Assessment of methods used in 1D models for computing bed-load transport in a large river: the Danube River in Slovakia." *Journal of Hydraulic Engineering*, 137(10), 1190–1199.

Camenen, B. and Larson, M. (2005). "A bedload sediment transport formula for the nearshore." *Estuarine, Coastal & Shelf Science*, 63, 249–260.

Camenen, B. and Larson, M. (2010). "Discussion of "measurements of sheet flow transport in acceleration-skewed oscillatory flow and comparison with practical formulations" by D.A. van der A, T.O'Donoghue and J.S. Ribberink." *Coastal Engineering*, 58(1), 131–134.

Chiew, Y.-M. and Parker, G. (1994). "Incipient sediment motion on non-horizontal slopes." *Journal of Hydraulic Research*, 32, 649–660.

Church, M., Hassan, M., and Wolcott, J. F. (1998). "Stabilizing self-organized structures in gravel-bed stream channels: Field and experimental observations." *Water Resources Research*, 34, 3169–3179.

Curran, J. C. (2007). "The decrease in shear stress and increase in transport rates subsequent to an increase in sand supply to a gravel-bed channel." *Sedimentary Geology*, 202(3), 572–580 Special issue: From Particle Size to Sediment Dynamics.

Dancey, C. L., Diplas, P., Papanicolaou, A., and Bala, M. (2002). "Probability of individual grain movementand threshold condition." *Journal of Hydraulic Engineering*, 128(12), 1069–1075.

Dey, S. (1999). "Sediment threshold." *Applied Mathematical Modelling*, 23(5), 399 – 417.

Dey, S. and Raju, U. V. (2002). "Incipient motion of gravel and coal beds." *Sãdhanã*, 27(5), 559–568.

Einstein, H. A. (1942). "Formulas for bed-load transportation." *Transactions of the American Society of Civil Engineering*, 107, 575–577.

Fenton, J. D. and Abbott, J. E. (1977). "Initial movement of grains on a stream bed: the effect of relative protrusion." *Proc. Royal Society of London, A*, 352, 523–537.

Garcia, M. (2008). *Sedimentation Engineering: Processes, Measurements, Modeling, and Practice*. Number 110 in ASCE manuals and reports on engineering practice. American Society of Civil Engineers, Reston, VA, USA.

Gregoretti, C. (2000). "The initiation of debris flow at high slopes: experimental results." *Journal of Hydraulic Research*, 38(2), 83–88.

Hassan, M., Saletti, M., Johnson, J., Ferrer-Boix, C., Venditti, J., and Church, M. (2020). "Experimental insights into the threshold of motion in alluvial channels: Sediment supply and streambed state.." *Journal of Geophysical Research: Earth Surface*, 125(e2020JF005736).

Haynes, H. and Pender, G. (2007). "Stress history effects on gravel bed stability." *Journal of Hydraulic Engineering*, 133(4), 343–349.

Hodge, R., Voepel, H., Leyland, J., Sear, D., and Ahmed, S. (2020). "X-ray computed tomography reveals that grain protrusion controls critical shear stress for entrainment of fluvial gravels." *Geology*, 48.

Hoffmans, G. J. C. M. (2010). "Stability of stones under uniform flow." *Journal of Hydraulic Engineering*, 136(2), 129–136.

Ikeda, H. and Iseya, F. (1988). "Experimental study of heterogeneous sediment transport." *Report No. 12*, Environmental Reserch Center, University of Tsukuba. 50pp.

Iwagaki, Y. (1956). "Fundamental study on critical tractive force." *Transaction of the Japanese Society of Civil Engineering*, 41, 1–21.

Jackson, W. L. and Beschta, R. L. (1984). "Influences of increased sand delivery on the morphology of sand and gravel channel." *J. American Water Resources Assoc.*, 20(4), 527–533.

Jain, R. K. and Kothyari, U. C. (2009). "Cohesion influences on erosion and bed load transport." *Water Resources Research*, 45.

JCGM (2008). “Evaluation of measurement data - Supplement 1 to the "Guide to the expression of uncertainty in measurement" - Propagation of distributions using a Monte Carlo method. ISO/IEC Guide 98-3-1.” *Report no.*, Joint Committee for Guides in Metrology.

Kim, S. C., Friedrichs, C. T., Maa, J. P. Y., and Wright, L. D. (2000). “Estimating bottom stress in tidal boundary layer from acoustic Doppler velocimeter data..” *Journal of Hydraulic Engineering*, 126(6), 399–406.

Kramer, H. (1935). “Sand mixtures and sand movement in fluvial models.” *Transactions of the American Society of Civil Engineering*, 100(1), 798–878.

Kuhnle, R., Wren, D., Langendoen, E., and Rigby, J. (2013). “Sand transport over an immobile gravel substrate.” *Journal of Hydraulic Engineering*, 139(2), 167–176.

Lajeunesse, E., Malverti, L., and Charru, F. (2010). “Bed load transport in turbulent flow at the grain scale: Experiments and modeling.” *Journal of Geophysical Research*, 115(F04001), 1–16.

Lamb, M. P., Dietrich, W. E., and Venditti, J. G. (2008). “Is the critical shields stress for incipient sediment motion dependent on channel-bed slope?.” *Journal of Geophysical Research*, 113(F02008), 20 p.

Lane, E. W. and Carlson, E. J. (1954). “Some observations on the effect of particle shape on the movement of coarse sediments.” *Transactions of the American Geophysical Union*, 35(3), 453–462.

Laronne, J. B. and Carson, M. A. (1976). “Interrelationships between bed morphology and bed-material transport for a small, gravel-bed channel.” *Sedimentology*, 23(1), 67–85.

Lavelle, J. W. and Mofjeld, H. O. (1987). “Do critical stress for incipient motion and erosion really exist?.” *Journal of Hydraulic Engineering*, 113(3), 370–385.

Le Coz, J., Renard, B., Bonnifait, L., Branger, F., and Le Boursicaud, R. (2014). “Combining hydraulic knowledge and uncertain gauging in the estimation of hydrometric rating curves: A Bayesian approach.” *Journal of Hydrology*, 509, 573–587.

Li, Z. and Komar, P. D. (1986). “Laboratory measurements of pivoting angle for applications to selective entrainment of gravel in a current..” *Sedimentology*, 33(3), 413–423.

584 Liu, Y., Métivier, F., Lajeunesse, E., Lancien, P., Narteau, C., Ye, B., and Meunier, P. (2008).
585 "Measuring bedload in gravel-bed mountain rivers: averaging> methods and sampling strate-
586 gies." *Geodinamica Acta*, 21(1-2), 81–92.
587 Mansanarez, V., Le Coz, J., Renard, B., Lang, M., Pierrefeu, G., and Vauchel, P. (2016). "Bayesian
588 analysis of stage-fall-discharge rating curves and their uncertainties." *Water Resources Research*,
589 52, 7424–7443.
590 Meyer-Peter, E. and Müller, R. (1948). "Formulas for bed-load transport." *Proc. 2nd IAHR*
591 *Congress*, Stockholm, Sweden, 39–64.
592 Mueller, E. R., Pitlick, J., and Nelson, J. M. (2005). "Variation in the reference shields stress for
593 bed load transport in gravel-bed streams and rivers." *Water Resources Research*, 41(W04006),
594 1–10.
595 Neill, C. and Yalin, M. (1969). "Quantitative definition of beginning of bed movement." *Journal*
596 *of Hydraulic Division*, 95(1), 585–588.
597 Paintal, A. S. (1971). "A stochastic model of bedload transport." *Journal of Hydraulic Research*,
598 9(4), 527–554.
599 Parker, G., Klingeman, P. C., and McLean, D. G. (1982). "Bed load and size distribution in paved
600 gravel-bed streams." *Journal of Hydraulic Division*, 108(HY4), 544–571.
601 Perret, E. (2017). "Transport of moderately sorted gravels at low bed shear stresses : impact of
602 bed arrangement and fine sediment inltration." Ph.D. thesis, Université Claude Bernard, Lyon1,
603 Lyon, France. 373p.
604 Perret, E., Berni, C., and Camenen, B. (2020). "How does bed surface impact bedload transport
605 over gravel-bed rivers?." *Earth Surface Processes & Landforms*, 45(5), 1181–1197.
606 Perret, E., Berni, C., Camenen, B., Herrero, A., and El Kadi Abderrezzak, K. (2018). "Transport of
607 moderately sorted gravel at low bed shear stresses: the role of fine sediment infiltration." *Earth*
608 *Surface Processes & Landforms*, 43, 1416–1430.
609 Perret, E., Renard, B., and Le Coz, J. (2021). "A rating curve model accounting for
610 cyclic stage-discharge shifts due to seasonal aquatic vegetation." *Water Resources Research*,

611 57(e2020WR027745).

612 Petit, F. (1989). “Evaluation des critères de mise en mouvement et de transport de la charge de fond
613 en milieu naturel..” *Bulletin de la Société Géographique de Liège*, 25, 91–111.

614 Petit, F., Gob, F., Houbrechts, G., and Assani, A. A. (2005). “Critical specific stream power in
615 gravel-bed rivers.” *Geomorphology*, 69, 92–101.

616 Pilotti, M. and Menduni, G. (2001). “Beginning of sediment transport of incoherent grains in
617 shallowshear flows.” *Journal of Hydraulic Research*, 39(2), 115–124.

618 Prancevic, J. P. and Lamb, M. P. (2015). “Unraveling bed slope from relative roughness in initial
619 sediment motion.” *Journal of Geophysical Research: Earth Surface*, 120, 474–489.

620 Rao, A. R. and Sitaram, N. (1999). “Stability and mobility of sand-bed channels affected by
621 seepage.” *Journal of Irrigation & Drainage Engineering*, 125(16), 370–379.

622 Recking, A. (2009). “Theoretical development on the effects of changing flow hydraulics on
623 incipient bedload motion.” *Water Resources Research*, 45, 1–16.

624 Recking, A. (2010). “A comparison between flume and field bedload transport data and
625 consequences for surface based bedload transport prediction.” *Water Resources Research*,
626 46(W03518), 1–16.

627 Recking, A., Frey, P., Paquier, A., Belleudy, P., and Champagne, J. Y. (2008). “Feedback between
628 bed load transport and flow resistance in gravel and cobble bed rivers.” *Water Resources Research*,
629 44(W05412), 1–21.

630 Reid, I., Frostick, L. E., and Layman, J. T. (1985). “The incidence and nature of bedload transport
631 during flood flows in coarse-grained alluvial channels.” *Earth Surface Processes & Landforms*,
632 10, 33–44.

633 Reid, I., Layman, J. T., and Frostick, L. E. (1980). “The continuous measurement of bedload
634 discharge.” *Journal of Hydraulic Research*, 18(3), 243–249.

635 Renard, B., Garreta, V., and Lang, M. (2006). “An application of Bayesian analysis and Markov
636 chain Monte Carlo methods to the estimation of a regional trend in annual maxima.” *Water*
637 *Resources Research*, 42(12 (W12422)), 1–17.

638 Roušar, L., Zachoval, Z., and Julien, P. (2016). "Incipient motion of coarse uniform gravel." *Journal*
639 *of Hydraulic Research*, 54(6), 615–630.
640 Shields, A. (1936). "Anwendung der Ahnlichkeits-mechanik und der turbulenzforschung auf die
641 geshiebebewegung [application of similarity principles and turbulence research to bed-load
642 movement]." *Preussische Versuchsanstalt fur Wasserbau und Schiffbau*, 26, 26 p. Berlin, Ger-
643 many (in German).
644 Shvidchenko, A. B. and Pender, G. (2000). "Flume study of the effect of relative depth on the
645 incipient motion of coarse uniform sediments." *Water Resources Research*, 36(2), 619–628.
646 Shvidchenko, A. B., Pender, G., and Hoey, T. B. (2001). "Critical shear stress for incipient motion
647 of sand/gravel streambeds." *Water Resources Research*, 37(8), 2273–2283.
648 Soulsby, R. L. and Whitehouse, R. J. S. W. (1997). "Threshold of sediment motion in coastal
649 environment." *Proc. Pacific Coasts and Ports'97 Conf.*, Christchurch, New Zealand, University
650 of Canterbury, 149–154.
651 Tait, S. (1993). "The physical processes of bed armouring in mixed grain sediment transport."
652 Ph.D. thesis, University of Aberdeen, Aberdeen.
653 U. S. Waterways Experiment Station (1935). "Studies of river bed materials and their movement
654 with special reference to the lower Mississippi River." *Report No. 17*, U. S. Army Corps of
655 Engineers, Vicksburg, Mississippi, U. S. A. 161 pp.
656 Vah, M., Khoury, A., Jarno, A., and Marin, F. (2022). "A visual method for threshold detection of
657 sediment motion in a flume experiment without human interference." *Earth Surface Processes*
658 *& Landforms*, 47, 1778–1789.
659 van Rijn, L. C. (1984). "Sediment transport, part I : bed load transport." *Journal of Hydraulic*
660 *Division*, 110(10), 1431–1456.
661 Vanoni, V. A. (1964). "Measurements of critical shear stress for entraining fine sediment in a
662 boundary layer. pasadena, california:." *Report No. KH-R-7*, W.M. Keck Laboratory of Hydraulics
663 and Water Resources, Division of Engineering and Applied Science, California Institute of
664 Technology, Passadena, California, USA.

Venditti, J. G., Nelson, P. A., Bradley, R. W., Haught, D., and Gitto, A. B. (2017). *Bedforms, Structures, Patches, and Sediment Supply in Gravel Bed Rivers*. D. Tsutsumi and J.B. Laronne.

Vericat, D., Church, M., and Batalla, R. J. (2006). "Bed load bias: Comparison of measurements obtained using two (76 and 152 mm) Helley-Smith samplers in a gravel bed river.." *Water Resources Research*, 42, 1–13.

Wilcock, P. R. (1988). "Methods for estimating the critical shear stress of individual fractions in mixed-size sediment." *Water Resources Research*, 24(7), 1127–1135.

Wilcock, P. R. (1996). "Estimating local bed shear stress from velocity observations." *Water Resources Research*, 32, 3361–3366.

Wilcock, P. R. and Crowe, J. C. (2003). "Surface-based transport model for mixed-size sediment." *Journal of Hydraulic Engineering*, 129(2), 120–128.

Wren, D., Kuhnle, R., Langendoen, E., and Rigby, J. (2014). "Turbulent flow and sand transport over a cobble bed in a laboratory flume." *Journal of Hydraulic Engineering*, 140(4), 167–176.

Yager, E. M., Schmeeckle, M. W., and Badoux, A. (2018). "Resistance is not futile: Grain resistance controls on observed critical shields stress variations." *Journal of Geophysical Research: Earth Surface*, 123, 3308–3322.

Young, R. A. and Mann, R. (1985). "Erosion velocities of skeletal carbonate sands, St. Thomas, Virgin Islands." *Marine Geology*, 69, 171–185.

APPENDIX I. EQUATIONS FOR THE COMPUTATION OF BED SHEAR STRESS

In Tab. 1 are the main methods for computing bed shear stress presented.

TABLE 1. Existing methods for the computation of bed shear stress.

Methods	Principle	Associated equations	Comments
Depth-slope	Basic resistance equation for open-channel uniform flow	$\tau = \rho g R_h J \approx \rho g h S$ (10)	Reach averaged method
Friction law	Calculation of τ based on a friction law	$\tau = \rho C_D U^2$ (11) $C_D = \left(\frac{\kappa}{1+\ln(Z_0/h)}\right)^2$ (12)	U local or V global, $Z_0 = k_s/30$ with $k_s = 2\ d_{90}$
Velocity profile analysis	Linear fit of the velocity profile in the log-region	$\frac{\bar{u}(z)}{u_*} = \frac{1}{\kappa}\ln\left(\frac{z}{Z_0}\right)$ (13)	Method accuracy depending on dataset quality for $\bar{u}(z)$
Reynolds stress analysis	Extrapolation of the linear part of the time-average turbulent velocity profile $-\overline{u'w'}$	$u_*^2 = \left[-\overline{u'w'}\right]_{(z=Z_b)}$ (14) $\tau = \tau_\nu + \tau_t = \mu\frac{\mathrm{d}\bar{u}}{\mathrm{d}z} - \rho\overline{u'w'}$ (15)	Viscous effect negligible outside the boundary layer ($\tau_\nu \approx 0$)
Turbulent kinetic energy analysis (TKE)	Extrapolation of the TKE profile to the bed level	$\lvert u_*\rvert = \sqrt{C_1\ [TKE]_{z=Z_b}}$ (16) $TKE = 0.5\left(\overline{u'^2} + \overline{v'^2} + \overline{w'^2}\right)$ (17)	C_1 is a constant (C_1=0.2)
1D BSV equation	Resolution of the 1D Barré-de-Saint-Venant (BSV) equation	$u_*^2 = Shg + (U\frac{\partial h}{\partial t} - h\frac{\partial U}{\partial t}) - gh\frac{\partial h}{\partial x}(1-Fr^2)$ (18)	For steady and uniform flows, Eq. 18 reduces to Eq. 10

J the energy slope, S longitudinal bed slope, R_h the hydraulic radius, C_D the friction coefficient, Z_0 the roughness length, $\bar{u}(z)$ the time-averaged velocity profile, $u_* = \sqrt{\tau/\rho}$ the friction velocity, $\kappa = 0,4$ the Von Karman constant, z the vertical component, u', v', and w' the measured turbulent velocities in x, y, and z-direction, respectively, z_b the bed level, τ_ν the viscous-shear, τ_t the turbulent-shear, μ the dynamic viscosity, t the time, Fr $= U/\sqrt{gh}$ the Froude number, U the depth-averaged velocity, and V the section-averaged velocity.

APPENDIX II. EQUATIONS FOR BAYESIAN ESTIMATION

The posterior pdf of unknown parameters $(\boldsymbol{\nu}, \sigma)$ given the observed dataset $\boldsymbol{O}$ can be computed as follows:

$$\underbrace{p\left(\boldsymbol{\nu}, \sigma | \boldsymbol{O}\right)}_{\text{posterior pdf}} \propto \underbrace{p\left(\boldsymbol{O} | \boldsymbol{\nu}, \sigma\right)}_{\text{likelihood}} \underbrace{p\left(\boldsymbol{\nu}, \sigma\right)}_{\text{prior pdf}} \tag{19}$$

where the symbol $\propto$ means 'is proportional to'. The likelihood results from the error model in equation (8) and can be computed as follows:

$$p\left(\boldsymbol{O} | \boldsymbol{\nu}, \sigma\right) = \prod_{i=1}^{n} f_{\mathcal{N}}\left(\theta_{cr,i}; M\left(d_{*,i}, S_i; \boldsymbol{\nu}\right), \sqrt{\sigma^2 + \Delta_{\theta_{cr},i}^2}\right) \tag{20}$$

where $f_{\mathcal{N}}(z; m, s)$ denotes the pdf of the normal distribution with mean m and standard deviation s, evaluated at value z.

The prior pdf is computed as:

$$p\left(\boldsymbol{\nu}, \sigma\right) = f_{\mathcal{U}}\left(\sigma; a, b\right) \prod_{k=1}^{p} f_{\mathcal{N}}\left(\nu_k; m_k, s_k\right) \tag{21}$$

where $f_{\mathcal{U}}$ denotes the pdf of a uniform distribution between a and b and the $f_{\mathcal{N}}$ terms in the product denote the pdf of the normal distribution used as prior for each parameter, as described in section 3.

APPENDIX III. PREDICTING CAPABILITIES OF θ_{CR} EQUATIONS

The following Figs. 8 and 9 presents the results for the predicting capabilities of the different equations presented in the document

Tab. 5 presents the statistical results as Tab. 5 but with an emphasis on the methodology used to evaluate τ_{cr}, i.e., using a reference transport rate or a visual definition, and the type of data, i.e., laboratory or field.

APPENDIX IV. IMPACT DATA UNCERTAINTY ON RESULTS

Fig. 10 presents the impact of the data average uncertainty $\overline{\Delta\theta_{cr}}$ on the parameter estimation for each model.

For Eq. 3 (Fig. 10a), the estimated model coefficients $\nu_1^{(1)}$, $\nu_2^{(1)}$, and $\nu_3^{(1)}$ decrease when data uncertainty increases, i.e., with a smaller sensitivity of Eq. 3 to grain size. For Eq. 4 (Fig. 10b), while the coefficient $\nu_1^{(2)}$ is independent of data uncertainty, $\nu_2^{(2)}$ decreases with larger uncertainty, indicating somehow a smaller impact of the less numerous data for high slopes. For Eq. 5 (Fig. 10c), one can observe a minimum and a maximum at our reference evaluation of the data uncertainty for $\nu_2^{(3)}$ and $\nu_4^{(3)}$, respectively.

List of Figure captions

Figure 1 : Uncertainty $u_{\theta_{cr}}$ as a function of the dimensionless grain size d_* (*def1*: reference transport rate, *def2*: visual definition).

Figure 2: Diagram of the Bayesian model to evaluate the critical Shields number: inputs, parameters, observations, and outputs.

Figure 3 : Critical Shields parameter θ_{cr} for inception motion estimated using Eq. 3 *versus* dimensionless grain size d^*; Uncertainty envelopes for parametric (E_{par}) and total uncertainty (E_{tot}) were defined as 95 % credibility intervals (E_{tot}=E_{par} + E_{struc}, with E_{struc} the structural uncertainty).

Figure 4 : Critical Shields parameter θ_{cr} for inception motion estimated using Eq. 4 *versus* longitudinal bed slope S; Uncertainty envelopes for parametric (E_{par}) and total uncertainty (E_{tot}) were defined as 95 % credibility intervals.

Figure 5 : Critical Shields parameter θ_{cr} for inception motion estimated using Eq. 5 *versus* dimensionless grain size d^* for different values of slope: $S = 0.001$ (a), $S = 0.02$ (b), $S = 0.1$ (c), and $S = 0.2$ (d); Uncertainty envelopes for the parametric (E_{par}) and total uncertainty (E_{tot}) were defined as 95 % credibility intervals.

Figure 6 : Evaluation of the total and parametric uncertainties in the models as function of the averaged uncertainties $\Delta\theta_{cr}$ in experimental data (For $\hat{\theta}_{cr}^{(3)}$, (a): $S = 0.001$, (b): $S = 0.02$, (c): $S = 0.10$, (d): $S = 0.20$).

Figure 7 : Critical Shields parameter θ_{cr} for inception motion estimated using Eq. 9 *versus* dimensionless grain size d^* for different values of slope: $S = 0.001$ (a), $S = 0.02$ (b), $S = 0.1$ (c), and $S = 0.2$ (d); Uncertainty envelopes for parametric (E_{par}) and total uncertainty (E_{tot}) were defined as 95 % credibility intervals.

Figure 8 : Predicted $\theta_{cr,eq}$ versus measured $\theta_{cr,exp}$ values of θ_{cr} using Eq. 3 with Soulsby and Whitehouse (1997) coefficients (a) or with the coefficient estimated with the Bayesian approach (b) and Eq. 4 with Recking (2009) coefficients (c) or with the coefficient estimated with the Bayesian

approach (d).

Figure 9 : Predicted $\theta_{cr,eq}$ versus measured $\theta_{cr,exp}$ values of θ_{cr} using Eq. 6 (a), Eq. 5 (b), and Eq. 9 (c).

Figure 10 : Boxplots of parameter estimations for Eqs. 3 (a), 4 (b), and 5 (c) depending on average uncertainties $\overline{\Delta\theta_{cr}}$ in experimental data.

List of Tables

TABLE 2. Estimation of each component of the uncertainty depending on the type of data.

Component	Laboratory data	Field data
Δ_{def}	Δ_{def1} = 10 %	Δ_{def1} = 20 %
	Δ_{def1} = 20 %	Δ_{def2} = 30 %
Δ_{τ}	$\Delta_{\tau,DS}$ = 15 %	$\Delta_{\tau,DS}$ = 30 %
	$\Delta_{\tau,FL}$ = 12 %	-
	$\Delta_{\tau,VP}$ = 10 %	-
	$\Delta_{\tau,TP}$ = 8 %	-
	$\Delta_{\tau,BSV}$ = 10 %	-

def1: reference transport rate, *def*2: visual definition, DS: depth-slope, FL: friction law, VP: velocity profile analysis, TP: turbulent profile analysis, BSV: 1D Saint Venant equation

TABLE 3. Prior specifications of the empirical parameters for the models (k = 1 to 4) discussed in this paper.

Equations	(m, s)-values for each parameter				
	$\nu_1^{(k)}$	$\nu_2^{(k)}$	$\nu_3^{(k)}$	$\nu_4^{(k)}$	$\nu_5^{(k)}$
$\widehat{\theta}_{cr}^{(1)}$ (Eq. 3)	$(0.24, 0.1)$	$(0.055, 0.02)$	$(-0.02, 0.01)$		
$\widehat{\theta}_{cr}^{(2)}$ (Eq. 4)	$(0.3, 0.1)$	$(0.04, 0.02)$			
$\widehat{\theta}_{cr}^{(3)}$ (Eq. 5)	$(0.3, 0.1)$	(1,0.5)	$(0.24, 0.05)$	$(0.055, 0.02)$	$(-0.02, 0.01)$
$\widehat{\theta}_{cr}^{(4)}$ (Eq. 9)	$(0.3, 0.1)$	(1,0.5)	$(0.24, 0.05)$	$(0.055, 0.02)$	

TABLE 4. Statistics on the proposed equations to estimate the critical Shields number.

Equations	parameters	$E_{r,20}$	$E_{r,50}$	mean$_{log}$	std$_{log}$
Eq. 3 (SW)	$\nu_1^{(1)} = 0.24$, $\nu_2^{(1)} = 0.055$, $\nu_3^{(1)} = -0.02$	29.0	59.5	0.043	0.237
Eq. 3 (Paper)	$\nu_1^{(1)} = 0.196$, $\nu_2^{(1)} = 0.0405$, $\nu_3^{(1)} = -0.0352$	33.1	64.5	-0.035	0.232
Eq. 4 (Rec)	$\nu_1^{(2)} = 0.3$, $\nu_2^{(2)} = 0.04$	37.1	67.4	-0.010	0.239
Eq. 4 (Paper)	$\nu_1^{(2)} = 0.327$, $\nu_2^{(2)} = 0.0352$	38.5	69.1	-0.053	0.239
Eq. 6 (Cam)		27.9	57.8	-0.099	0.225
Eq. 5 (Paper)	$\nu_1^{(3)} = 1.055$, $\nu_2^{(3)} = 0.274$, $\nu_3^{(3)} = 0.510$, $\nu_4^{(3)} = 0.134$, $\nu_5^{(3)} = -0.068$	37.7	68.7	-0.040	0.206
Eq. 9 (Paper, Section 5)	$\nu_1^{(4)} = 1.158$, $\nu_2^{(4)} = 0.180$, $\nu_3^{(4)} = 0.410$, $\nu_4^{(4)} = 0.195$	42.1	71.0	-0.021	0.193

SW: Soulsby and Whitehouse (1997), Rec: Recking (2009), Cam: Camenen (2012), Paper: from this paper.

TABLE 5. Statistics on the proposed equations to estimate the critical Shields number for selected parts of the data set.

Equations	$E_{r,20}$	$E_{r,50}$	mean$_{log}$	std$_{log}$
reference transport rate				
Eq. 3 (SW)	38.6	68.7	0.014	0.215
Eq. 3 (Paper)	32.2	66.0	-0.069	0.211
Eq. 4 (Rec)	47.1	75.7	-0.003	0.177
Eq. 4 (Paper)	42.2	76.6	-0.045	0.176
Eq. 6 (Cam)	26.1	56.5	-0.121	0.204
Eq. 5 (Paper)	38.3	71.1	-0.069	0.186
Eq. 9 (Paper)	45.3	74.2	-0.053	0.178
visual observations				
Eq. 3 (SW)	23.6	54.5	0.059	0.247
Eq. 3 (Paper)	33.6	63.7	-0.016	0.241
Eq. 4 (Rec)	31.5	62.7	-0.014	0.268
Eq. 4 (Paper)	36.4	64.9	-0.057	0.267
Eq. 6 (Cam)	28.8	58.5	-0.087	0.235
Eq. 5 (Paper)	37.4	67.3	-0.024	0.215
Eq. 9 (Paper)	40.3	69.3	-0.003	0.199
laboratory data				
Eq. 3 (SW)	29.1	60.5	0.035	0.233
Eq. 3 (Paper)	33.8	65.1	-0.041	0.228
Eq. 4 (Rec)	38.2	68.3	-0.017	0.236
Eq. 4 (Paper)	39.5	69.7	-0.059	0.236
Eq. 6 (Cam)	27.8	57.9	-0.104	0.224
Eq. 5 (Paper)	38.4	69.5	-0.044	0.201
Eq. 9 (Paper)	43.1	72.4	-0.025	0.186
field data				
Eq. 3 (SW)	25.9	44.4	0.165	0.273
Eq. 3 (Paper)	22.2	55.6	0.062	0.277
Eq. 4 (Rec)	18.5	51.9	0.091	0.266
Eq. 4 (Paper)	22.2	59.3	0.046	0.263
Eq. 6 (Cam)	29.6	55.6	-0.026	0.226
Eq. 5 (Paper)	27.8	55.6	0.032	0.270
Eq. 9 (Paper)	25.9	50.0	0.044	0.280

SW: Soulsby and Whitehouse (1997), Rec: Recking (2009), Cam: Camenen (2012), Paper: from this paper.

List of Figures

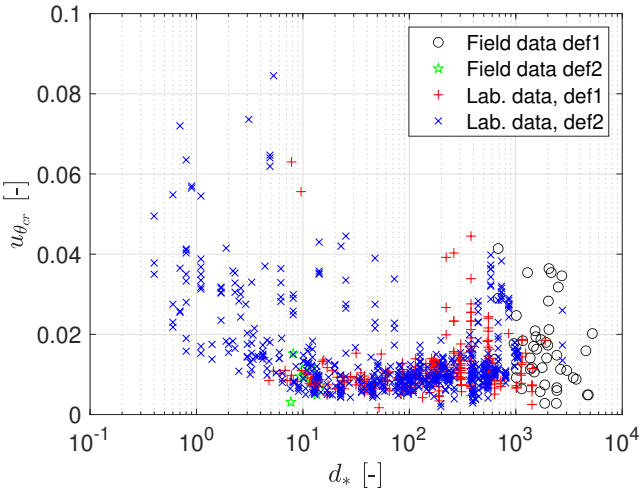

Fig. 1. Uncertainty $u_{\theta_{cr}}$ as a function of the dimensionless grain size d_* (*def1*: reference transport rate, *def2*: visual definition).

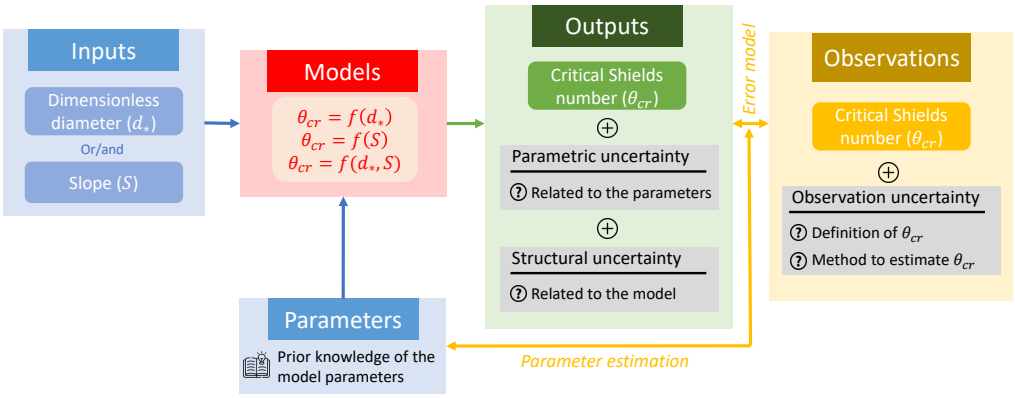

Fig. 2. Diagram of the Bayesian model to evaluate the critical Shields number: inputs, parameters, observations, and outputs.

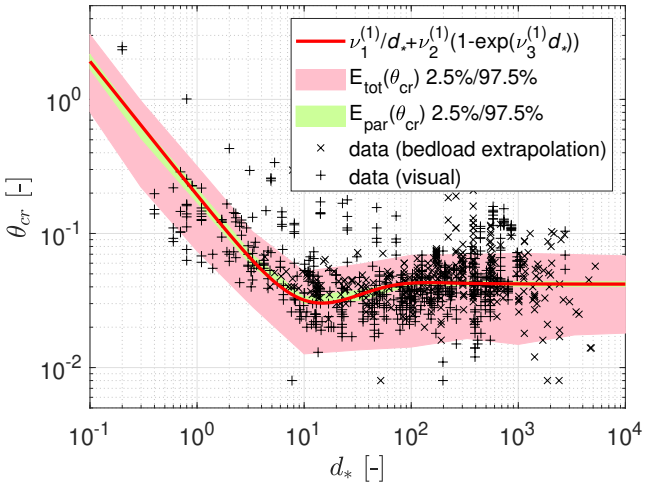

Fig. 3. Critical Shields parameter θ_{cr} for inception motion estimated using Eq. 3 *versus* dimensionless grain size d^*; Uncertainty envelopes for parametric (E_{par}) and total uncertainty (E_{tot}) were defined as 95 % credibility intervals (E_{tot}=E_{par} + E_{struc}, with E_{struc} the structural uncertainty).

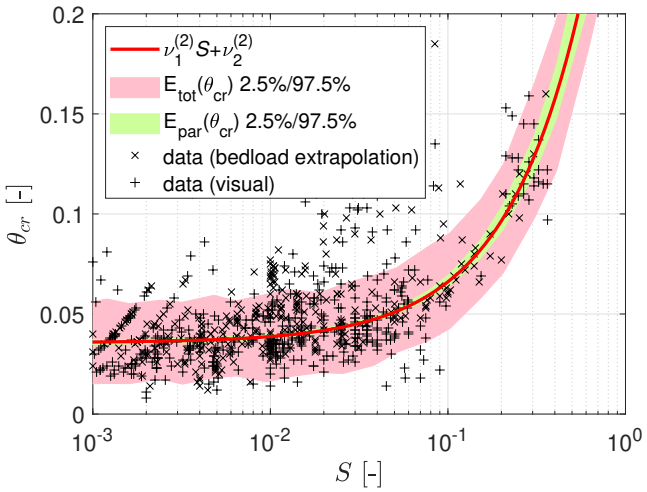

Fig. 4. Critical Shields parameter θ_{cr} for inception motion estimated using Eq. 4 *versus* longitudinal bed slope S; Uncertainty envelopes for parametric (E_{par}) and total uncertainty (E_{tot}) were defined as 95 % credibility intervals.

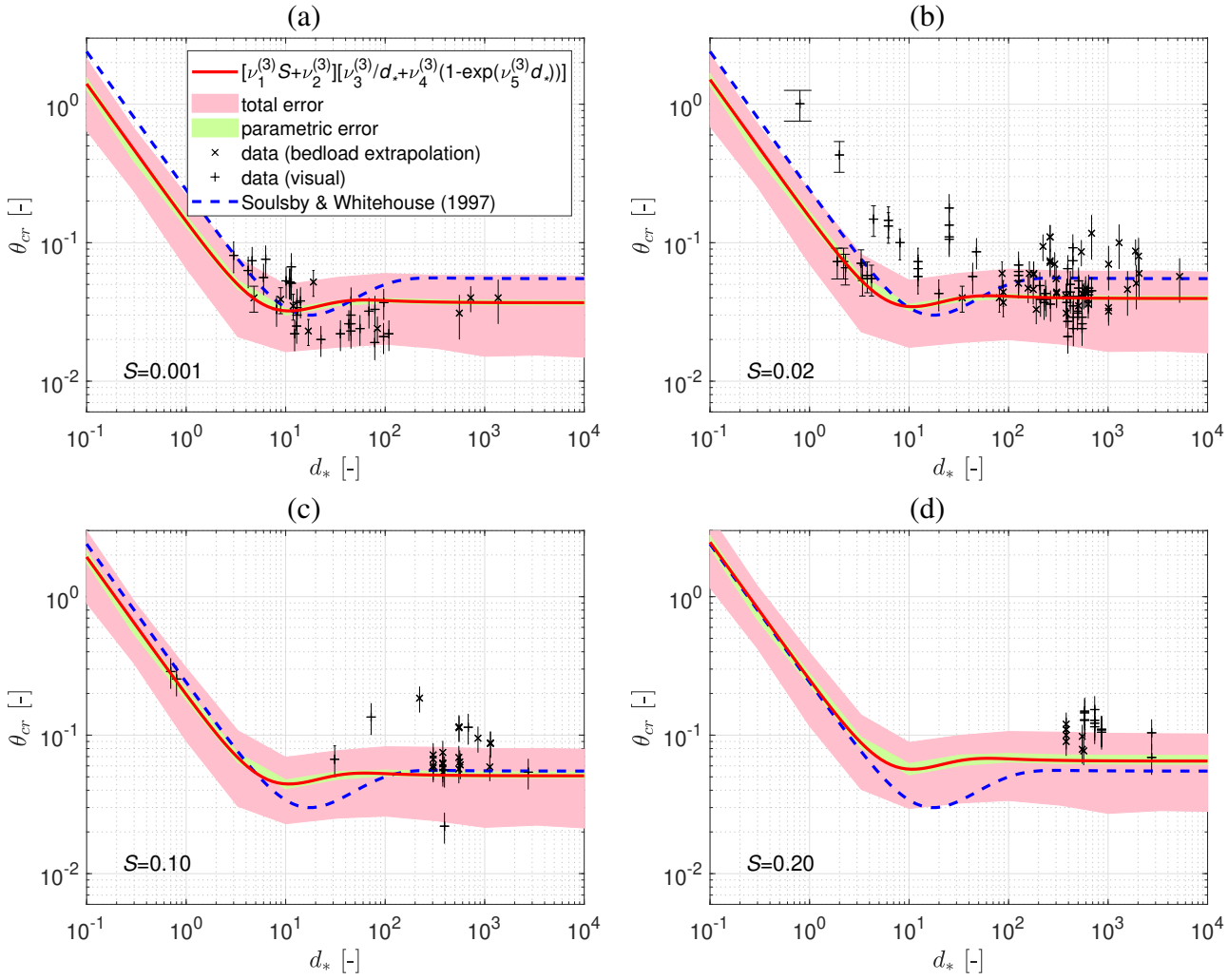

Fig. 5. Critical Shields parameter θ_{cr} for inception motion estimated using Eq. 5 *versus* dimensionless grain size d^* for different values of slope: $S = 0.001$ (a), $S = 0.02$ (b), $S = 0.1$ (c), and $S = 0.2$ (d); Uncertainty envelopes for the parametric (E_{par}) and total uncertainty (E_{tot}) were defined as 95 % credibility intervals.

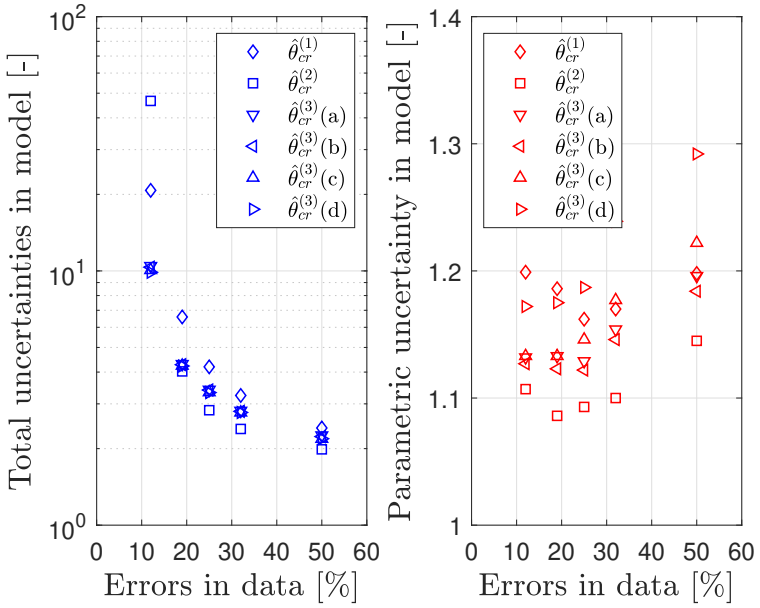

Fig. 6. Evaluation of the total and parametric uncertainties in the models as function of the averaged uncertainties $\Delta\theta_{cr}$ in experimental data (For $\hat{\theta}_{cr}^{(3)}$, (a): $S = 0.001$, (b): $S = 0.02$, (c): $S = 0.10$, (d): $S = 0.20$).

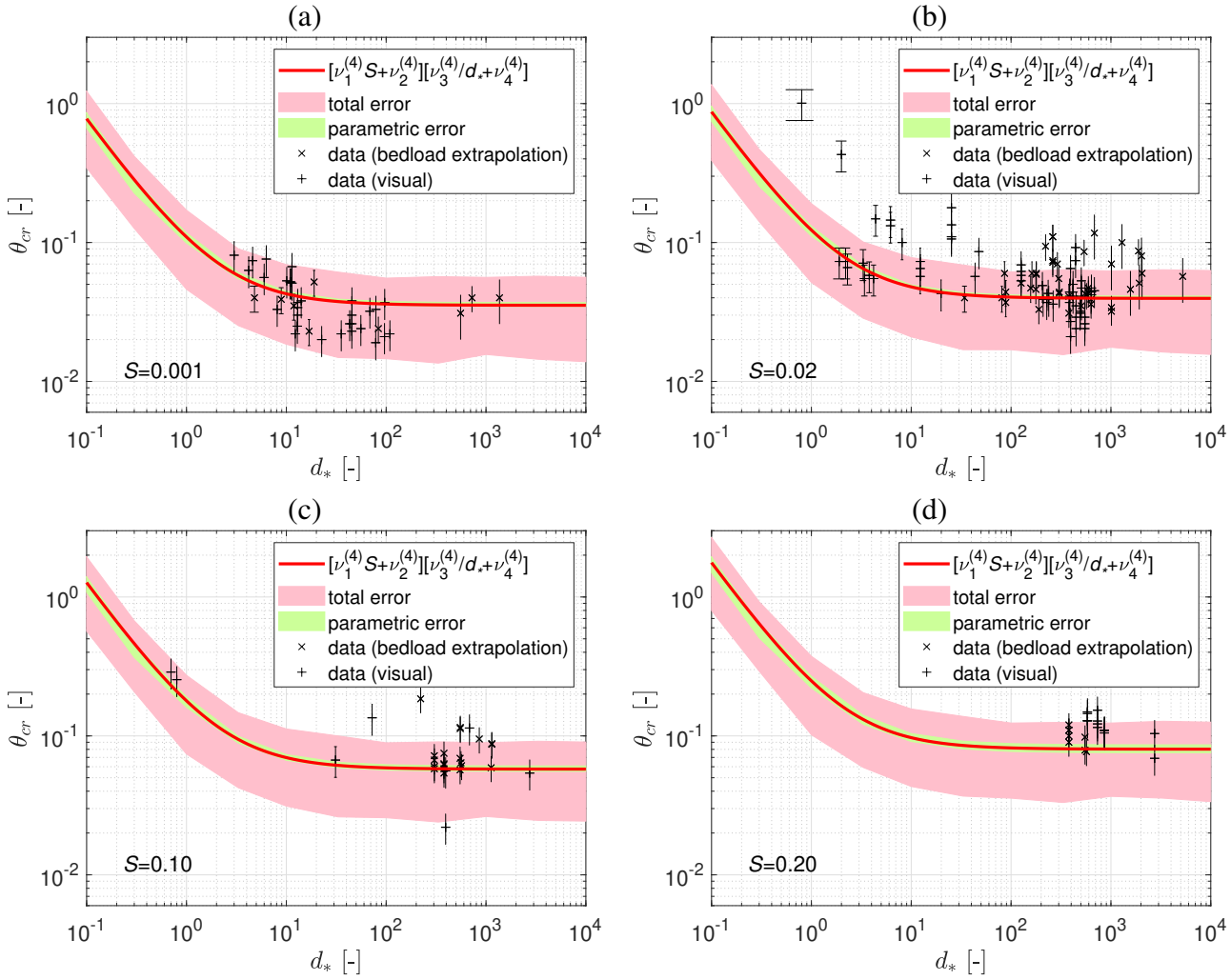

Fig. 7. Critical Shields parameter θ_{cr} for inception motion estimated using Eq. 9 *versus* dimensionless grain size d^* for different values of slope: S = 0.001 (a), S = 0.02 (b), S = 0.1 (c), and S = 0.2 (d); Uncertainty envelopes for parametric (E_{par}) and total uncertainty (E_{tot}) were defined as 95 % credibility intervals.

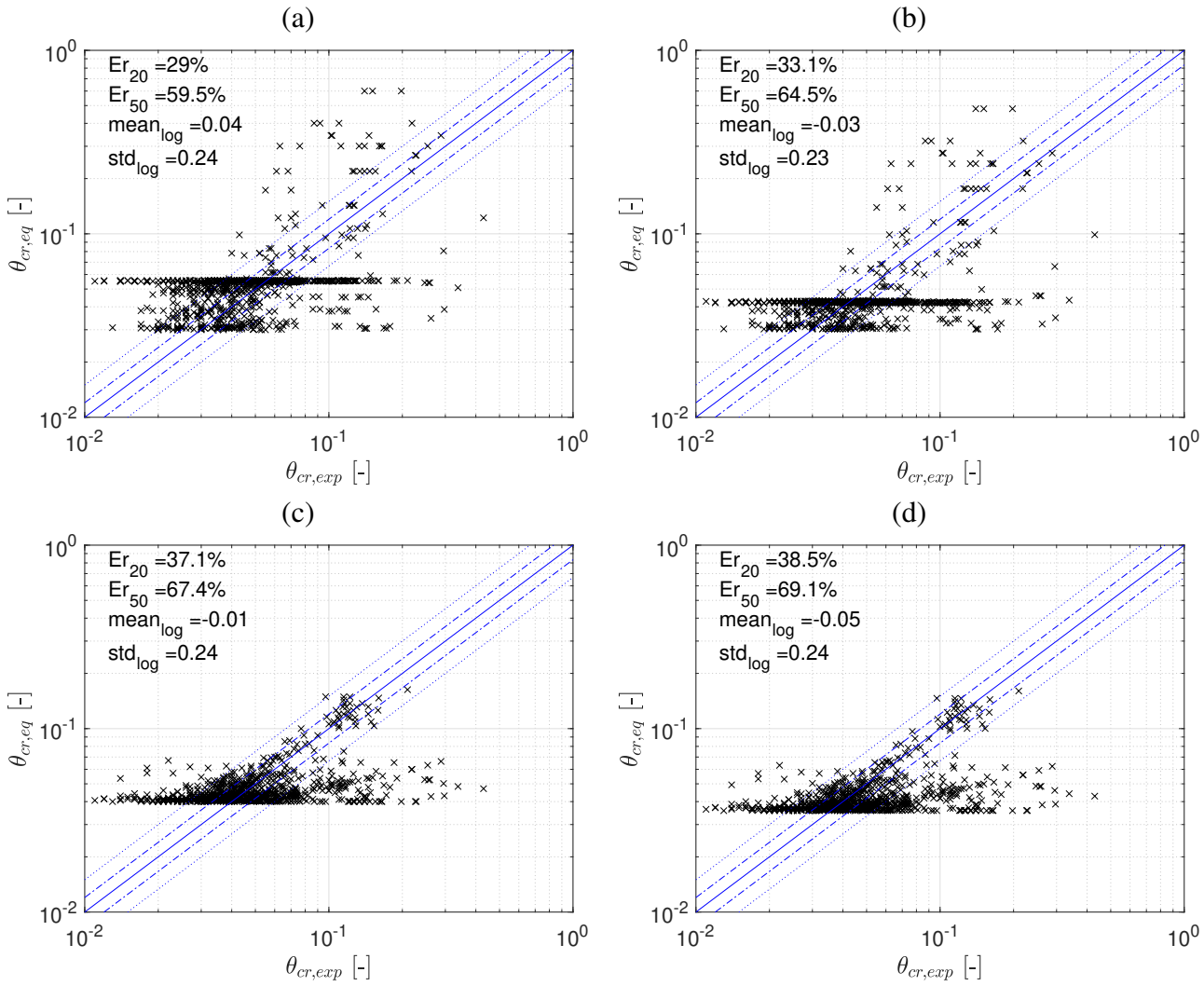

Fig. 8. Predicted $\theta_{cr,eq}$ versus measured $\theta_{cr,exp}$ values of θ_{cr} using Eq. 3 with Soulsby and Whitehouse (1997) coefficients (a) or with the coefficient estimated with the Bayesian approach (b) and Eq. 4 with Recking (2009) coefficients (c) or with the coefficient estimated with the Bayesian approach (d).

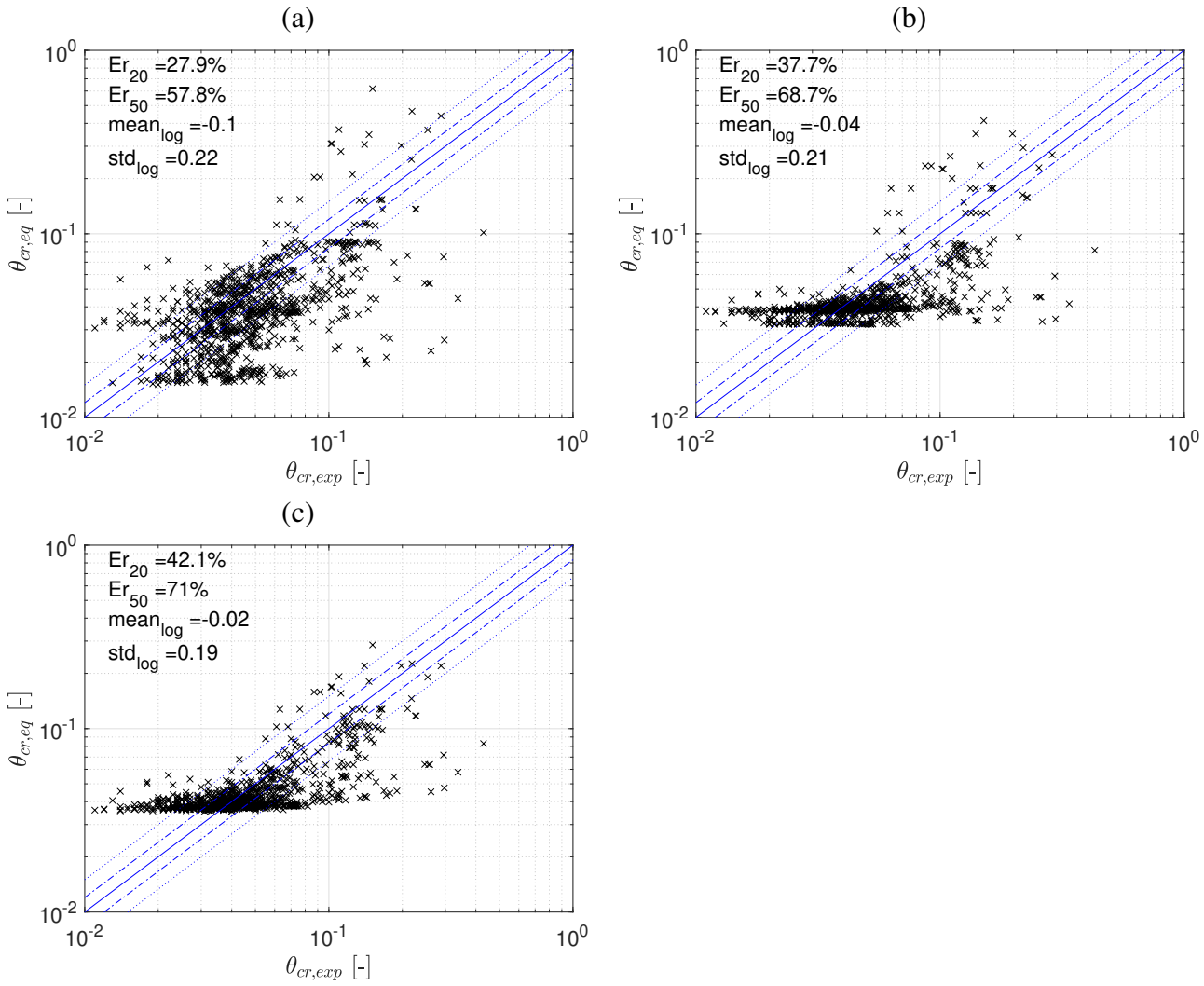

Fig. 9. Predicted $\theta_{cr,eq}$ versus measured $\theta_{cr,exp}$ values of θ_{cr} using Eq. 6 (a), Eq. 5 (b), and Eq. 9 (c).

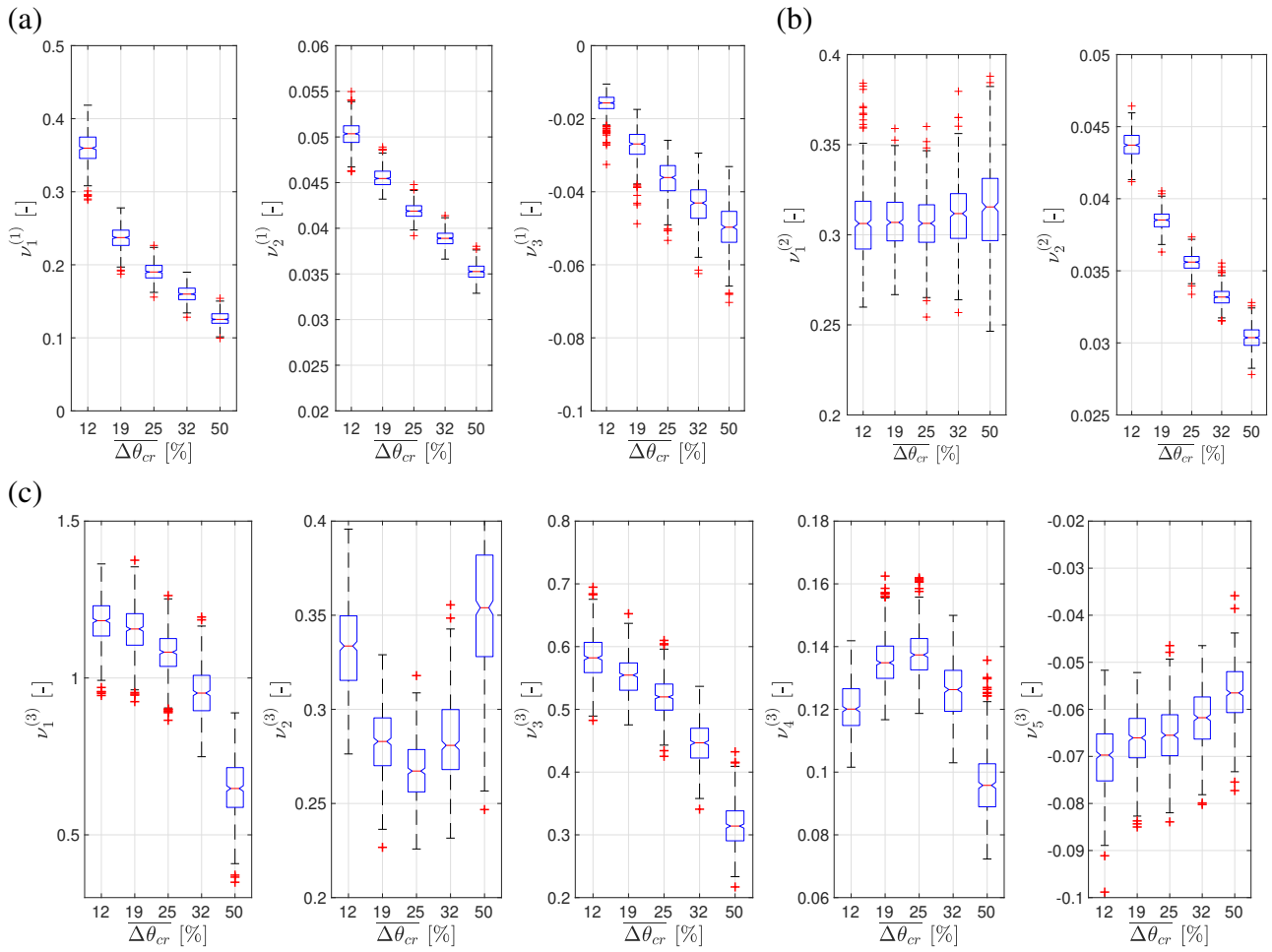

Fig. 10. Boxplots of parameter estimations for Eqs. 3 (a), 4 (b), and 5 (c) depending on average uncertainties $\overline{\Delta\theta_{cr}}$ in experimental data.